SB³C2020
Summer Biomechanics, Bioengineering and Biotransport Conference
June 17-20, Vail, CO, USA

ANISOTROPIC MATERIAL PROPERTIES OF THE HUMAN UTERUS

S. Fang (1), J. McLean (2), J. Vink (3), C. Hendon (2), K. Myers (1)

(1) Department of Mechanical Engineering
Columbia University
New York, NY, USA

(2) Department of Electrical Engineering
Columbia University
New York, NY, USA

(3) Department of Obstetrics and Gynecology
Columbia University Medical Center
New York, NY, USA

INTRODUCTION

The mechanical function of the uterus is crucial for protection of the fetus during a healthy pregnancy. Throughout gestation, the uterine wall remains in a passive state and accommodates the expanding amniotic sac by growing, unfolding, and stretching. Then—ideally at term (defined as 37 weeks)—the onset of labor triggers a functional change: the tissue becomes highly contractile to safely deliver the baby. Early contractile activation of uterine tissue can lead to preterm labor and birth (PTB). In 2014, 9.56 percent of pregnancies ended in PTB; it is also the leading cause of death in children under five years of age [1]. Characterizing the material properties of uterine tissue is important for understanding mechanical failures of the uterus and the causes of PTB.

Previous uniaxial dynamic tensile tests were performed to obtain the uterine material properties [2]. Indentation tests followed by finite element modeling (FEM) have been employed to characterize the mechanical anisotropy of human cervical tissue [3]. The goal of this research is to use mechanical indentation tests and FEM, to characterize the mechanical anisotropy of the human uterus.

METHODS

Specimen preparation: 78 uterine specimens were collected from consenting 28 patients who underwent hysterectomy. 40 specimen slices of 6 uteri were tested and presented in this study. Patient ages ranged from 39 to 49 at the time of collection, with various recorded obstetric histories (parity range: 0 to 12). Immediately after hysterectomy, a specimen was collected from each of three uterine locations: anterior, posterior, and fundus. All specimens spanned the width of the uterine wall (15 to 25 mm) and covered a square cross-sectional area with an edge length between 10 and 15 mm. All specimens were flash frozen using dry ice immediately after collection and stored in a –80°C freezer prior to mechanical testing. Before each test, the specimens were thawed at room temperature for 2 hours in phosphate-buffered saline (PBS). Then each specimen was divided into 4 to 8 slices parallel to the uterine wall. The thickness of each slice ranged from 3 to 6 mm. Masson Tri-chrome stained histology was also performed on selected slices to investigate the tissue composition.

Mechanical testing: Each slice was dried using KimWipes and speckled with Verhoeff's stain using an airbrush. After speckling, the slice was positioned in the bath chamber of a custom experiment rig (Fig. 1A) and submerged in PBS. The rig was then placed on the rigid surface of a universal testing machine (Instron, Inc., Norwood, MA). Indentation tests were performed using a 6-mm diameter spherical indenter attached to a 5N load cell.

A four-level ramp-hold indentation test was performed (Fig. 1B). Indentation depths were prescribed as percent displacement from total specimen thickness at the indentation location. For slices with thickness more than 5 mm, indentation depths were 12.5, 25, 37.5, and 50 percent; for thinner specimens, indentation depths were 15, 30, 45, and 60 percent. For all slices, the ramping rate was 1 percent per second. After each ramp, the indenter was held for 480, 600, 720, and 900 seconds, respectively, in order for the tissue to equilibrate. Force-time data were collected using material tester software (Instron, Inc., Blue Hill).

Digital image correlation (DIC): The DIC algorithm identifies unique pattern features within small pixel subsets. By tracking them, it estimates displacement and corresponding strain. The specimens sat on top of the rig's acrylic window surface. Below the window, a 90-deg prism was fixed to reflect the specimen bottom surface into a camera to capture the full-field displacement. Images were taken using Vic-Snap (Correlation Solutions, Irmo, SC). Calibration images were taken with a standard ruler in the field of view before starting each test set. The images were processed with Vic-2D (Correlated Solutions, v6, Irmo, SC) using an incremental correlation method. The displacement field

(in mm) was converted from the pixel field referencing the calibration images. Lagrange strains in horizontal (e_{xx}^{DIC}) and vertical (e_{yy}^{DIC}) directions were calculated using a 90% centered Gaussian filter and extracted.

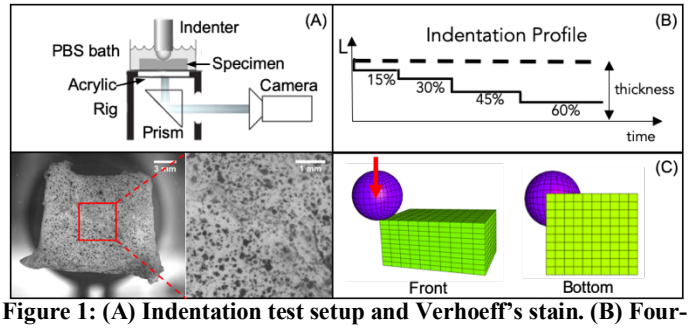

Figure 1: (A) Indentation test setup and Verhoeff's stain. (B) Four-level ramp-hold testing profile. (C) FEM front & bottom view.

Finite element analysis (FEA): FEA was run using the FEBio software suite. A rectangle representing a quadrant of the specimen was created based on its actual dimensions to decrease computational complexity, and a 6-mm diameter sphere was used to represent the indenter (Fig. 1C). These were meshed using HEX-8 elements. Sliding contact was assigned between the indenter and specimen. The specimen's bottom surface was fixed in the z dimension. Because of the quadrant model adaptation, fixed-displacement boundary conditions normal to the symmetry planes were applied. Four displacements were prescribed to represent the four-level ramp-hold protocol.

The material properties of the specimen were modeled as an anisotropic fiber composite. In this model, a continuously distributed fiber network was embedded in a compressible Neo-Hookean ground substance [3]. The total Helmholtz free energy density, ψ, is an additive contribution from the fibrous network, ψ^{FN}, and a ground substance of collagenous ECM, ψ^{GS},

$$\psi(\mathbf{F},\mathbf{n},b) = \psi^{FN}(\mathbf{F},\mathbf{n},b) + \psi^{GS}(\mathbf{F})$$

where **F** is the Cauchy-Green deformation tensor, **n** is the preferential fiber direction, and b is the von-Mises concentration factor [3]. Because the fiber bundles will have less tensile strain than the ECM between them, we assume that their preferential direction is perpendicular to the direction of principal strain as determined by DIC.

Inverse finite element analysis (IFEA): IFEA was performed to fit four material parameters to the experimental data: Young's Modulus E, Poisson's ratio ν, the fiber stiffness factor ξ, and the fiber angle concentration b. The following objective function was optimized to find the best-fit material parameters:

$$\Xi(E,\nu,\xi,b) = \sum_{i=1}^{N}\left|\frac{e_{xx}^{F^i} - e_{xx}^{E^i}}{e_{norm}^{E^n}}\right| + \sum_{i=1}^{N}\left|\frac{e_{yy}^{F^i} - e_{yy}^{E^i}}{e_{norm}^{E^n}}\right| + \sum_{i=1}^{N}\left|\frac{F^{F^i} - F^{E^i}}{F^{E^n}}\right|$$

where superscripts "F" and "E" denoted the force and strain data of the FEA and the experiment, respectively.

Computations were run on Columbia University's high-performance computer using a genetic algorithm (GA) with three operations (crossover, mutation, and selection). A total of 40 to 300 generations were iterated for each case until the error threshold (5%) was met. The fitting range of the parameters and the fitted results after the optimization are listed in Table 1. The fitting range was determined by both a comparison to a previous study on the cervix [3] and preliminary results from manual fitting prior to the optimization. The GA method was finally validated by comparing results with an exhaustive method for a subset of cases. The parameters fitted for each specimen were then compared across specimens along three dimensions: uterine layers, uterine locations, and patient parities.

Table 1: The fitting range and optimized results of the parameters of 40 slices from 6 patients.

Parameter	Range	Optimized Results (n=40)
E	$[10^{-4}, 10^{-1}]$ kPa	2.58 ± 1.90 kPa
ν	[0, 0.49]	0.39 ± 0.10
ξ	$[10^{-4}, 1]$ Pa	$0.91 \pm 1.40 \times 10^{-3}$ Pa
b	[0, 5]	2.94 ± 1.17

RESULTS

Young's Modulus E at the anterior wall of one NP uterus was significantly smaller than that at its posterior wall (Fig. 2A). Poisson's ratio ν at the perimetrium layer of one PG uterus was much smaller than that at its myometrium layer (Fig. 2B; variation in sample thickness affects the number of data points at each location). The vertical strain of the specimen bottom surface shows a good match between the experiment and FEA (Fig. 2C).

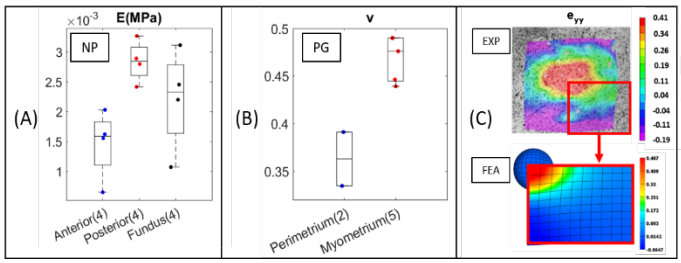

Figure 2: (A) Young's Modulus E at different locations of one NP uterus. (B) Poisson's ratio ν at different layers of one PG uterus. (C) The vertical strain (e_{yy}) from the experiment and the FEA.

DISCUSSION

In this study, a workflow of experiments and data processing techniques were employed to characterize the anisotropic material properties of the human uterus. Within each uterus, significant differences in Young's Modulus E and Poisson's ratio ν were observed at different locations and different layers, indicating the heterogeneity of the human uterine material properties. However, the fitted values for fiber stiffness ξ and angle concentration b exhibited a wide spread with no significant differences observed across comparison groups. There were also no obvious differences between patients with different parities, as suggested in previous studies [2].

The research and conclusions described in this abstract have the following limitations: the fiber concentration parameter b is not sensitive to this indentation testing method because more than one fiber family could potentially be in the same area of interest; differences between uteri could outweigh those induced by parity; and the material properties could be impacted by the tissue's pathological nature. Future work, especially the use of optical coherence tomography [4] and the analysis of more tissue samples, aims to address these shortcomings.

ACKNOWLEDGEMENTS

Research reported in this publication was supported by the NIH R01HD091153 to KM and R01HD072077 to TJH, HF & KM. The content is solely the responsibility of the authors and does not necessarily represent the official views of the NIH.

REFERENCES

[1] Martin, J. A., et al., *Statistics (Ber).,* 64(1):1–104, 2015.
[2] Manoogian, S.J., et al. *J Biomech* 45:1724–1727, 2012.
[3] Shi, L., et al., *J Biomech*, 141:091017, 2019.
[4] Yao, W., et al., *PLoS ONE,* 11(11): e0166709, 2016.